Journal of Biomedical Optics 15(5), 056008 (September/October 2010)

Photoacoustic and high-frequency power Doppler ultrasound biomicroscopy: a comparative study

Yan Jiang
Tyler Harrison
Janaka Ranasinghesagara
Roger J. Zemp
University of Alberta
Department of Electrical and Computer Engineering
Edmonton, Alberta T6G 2V4, Canada

Abstract. Both photoacoustic imaging and power Doppler ultrasound are capable of producing images of the vasculature of living subjects, however, the contrast mechanisms of the two modalities are very different. We present a quantitative and objective comparison of the two methods using phantom data, highlighting relative merits and shortcomings. An imaging system for combined photoacoustic and high-frequency power Doppler ultrasound microscopy is presented. This system uses a swept-scan 25-MHz ultrasound transducer with confocal dark-field laser illumination optics. A pulse-sequencer enables ultrasonic and laser pulses to be interlaced so that photoacoustic and power Doppler ultrasound images can be coregistered. Experiments are performed on flow phantoms with various combinations of vessel size, flow velocity, and optical wavelength. For the task of blood volume detection, power Doppler is seen to be advantageous for large vessels and high flow speeds. For small vessels with low flow speeds, photoacoustic imaging is seen to be more effective than power Doppler at the detection of blood as quantified by receiver operating characteristic analysis. A combination of the two modes could provide improved estimates of fractional blood volume in comparison with either mode used alone. [DOI: 10.1117/1.3491126]

Keywords: photoacoustic imaging; high-frequency ultrasound; power Doppler; flow phantom.

Paper 10120PRR received Mar. 10, 2010; revised manuscript received Aug. 9, 2010; accepted for publication Aug. 13, 2010; published online Sep. 30, 2010.

1 Introduction

Photoacoustic microscopy (PAM) is a hybrid imaging technique that combines high optical contrast and high ultrasonic spatial resolution at imaging depths much greater than optical microscopy methods.[1] When nanosecond-duration laser pulses are transmitted into biological tissues, wideband ultrasonic waves are emitted as a result of optically induced thermoelastic expansion. The magnitude of the received photoacoustic (PA) signal is proportional to optical absorption, the time of flight of the signal is proportional to depth of the absorbing structures, and the resolution is determined by ultrasonic detection considerations. Visualization of microvasculature is important to diagnose many diseases. Since blood is more absorbing than surrounding tissues at certain wavelengths, there is significant endogenous contrast available for PA imaging of microvascular structures. Maslov et al.[2] and Zhang et al.[3] have demonstrated a dark-field confocal PAM system for subcutaneous microvasculature visualization. Moreover, with known absorption spectra of oxy- and deoxyhemoglobin, PAM can be used to image blood oxygen saturation (sO_2) as well as relative concentration of total hemoglobin (C_{HB}). This has been demonstrated by Zhang et al.[3,4] among others.

Power Doppler ultrasound imaging is a technique that displays the backscatter strength of moving blood to identify regions of blood flow. This is in contrast to color Doppler ultrasound, a method to estimate and image blood flow speed and direction. The intensity of power Doppler images is proportional to the number of scatterers moving within a vascular volume, rather than the frequency shifts they generate,[5] which means that power Doppler is irrespective of Doppler angles between ultrasound beam and direction of flow. This feature improves the ability of imaging tortuous and irregular blood vessels. While clinical ultrasound systems operate in the 1- to 15-MHz range,[6] higher frequencies (20 to 100 MHz) have been aimed to provide finer spatial resolution. High-frequency (>20 MHz) power Doppler ultrasound has been used to assess microvascular density and angiogenesis in preclinical small animal models.[7] However, several limitations should be addressed when using this technique. First, tissues surrounding blood vessels often generate scattered signals much stronger than reflected signals from moving blood, so clutter filtering is necessary before Doppler power calculations. The performance of power Doppler imaging is dependent on subjective, rather than objective, wall filter parameters and display threshold levels. Second, in practice, tissues are not always stationary, and the movement of soft tissues causes signals of high intensity and low frequency. Since detection of

---

Address all correspondence to: Yan Jiang, University of Alberta, Department of Electrical and Computer Engineering, Edmonton, Alberta T6G 2V4, Canada. Tel: 780-492-9463. E-mail: yjiang5@ualberta.ca

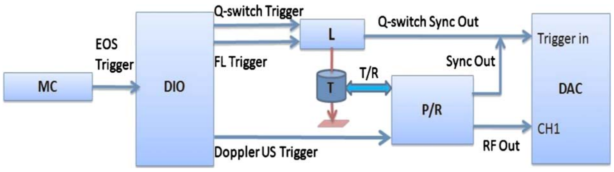

Fig. 1 Block diagram of the combined PA and Doppler ultrasound system: MC, motor controller; DIO, digital input-output card; L, laser; T, ultrasound transducer; P/R, ultrasound pulser/receiver; DAC, digital acquisition card; EOS: end-of-scan.

small blood vessels with slow flow velocities requires a low wall filter cutoff velocity, these clutter signals can survive wall filtering and create color pixel artifacts in power Doppler images. The blood volume fraction is hard to interpret in the presence of color pixel artifacts. On the other hand, while wall filters can reject clutter signals, some blood flow signals, especially from the slow velocity flows, can also be rejected. This may decrease the sensitivity of blood flow detection.

We developed a hybrid PA and high-frequency power Doppler ultrasound imaging system to provide coregistered PA and power Doppler images. Using this system to image flow phantoms, we developed a quantitative and objective methodology to compare the relative performance of power Doppler ultrasound and PA imaging. While various groups have performed PA and power Doppler imaging separately,[3,8] to our knowledge, no one has combined them and compared them in such a study. The combined system aims take advantage of both modalities to improve image quality of both macrovasculature (∼ hundreds of micrometers in diameter) and microvasculature and improve estimation of microvascular density. In this paper, the development of our combined system as well as signal processing strategies are described. Coregistered PA and power Doppler images acquired from flow phantoms with different combinations of vessel size and mean flow velocity are presented. Blood detection performance of each technique is evaluated by receiver operating characteristic analysis.

2 Methods

2.1 *Experimental System*

Figure 1 shows a block diagram of system instrumentation. The entire system can be controlled via a single computer. A combined light delivery and ultrasound probe is mounted on a voice coil positioning stage (VCS-10-023-BS-01, 1.0-in. travel, 2.3 lb continuous force, 6.9 lb peak force, purchased from H2W technologies, Inc., Valencia, California). This stage is driven by a programmed motor controller (Elmo Harmonica HAR 5/60, Elmo Motion Control Inc., Nashua, New Hampshire) to oscillate at fixed scanning speed. A digital output bit from the motor controller is set to high for a short duration at the end of each scan trajectory and sent to a digital input-output (DIO) card (NI PCI-6542, National Instruments, Inc). This end-of-scan (EOS) trigger is used to mark the beginning of an image frame and trigger the DIO card to generate a pulse sequence that is sent to the ultrasound pulser/receiver (5073PR, Panametrics, Waltham, Massachusetts) and/or laser. The ultrasound pulser/receiver is capable of a repetition rate up to 10 kHz, and can provide energy up to 16 μJ with amplifier gain up to 39 dB.

Currently, our system can provide several imaging modes, such as ultrasound (US) *B*-mode, PA mode and Doppler US mode. In PA mode, the DIO card is triggered by EOS output and then generates a pulse sequence to trigger the laser flashlamp and *Q*-switch. It was found that *Q*-switch triggering in addition to flashlamp (FL) triggering was important to reduce laser pulse timing jitter. A *Q*-switched Nd:YAG laser (Ultra UL 421111, Big Sky Technologies, Bozeman, Montana) with a maximum pulse repetition rate of 20 Hz was used to obtain a 10-ns pulse of 532-nm wavelength. To provide a longer wavelength, a tunable laser system was also used in this study. A tunable optical parametric oscillator (Surelite OPO Plus, Continuum, Santa Clara, California) was pumped by a *Q*-switched Nd:YAG laser (Surelite III, Continuum, Santa Clara, California) with repetition rate of 10 Hz. The tuning range is from 410 to 710 nm. PA and Doppler US modes are combined by using the DIO card to interleave laser and US triggers so that images can be coregistered.

Radio frequency (rf) data received by the US pulser/receiver is digitized by an eight-chanel PCI (peripheral component interconnect) data acquisition card (CS22G8, Gage Cobra, Gage Applied Systems, Inc.) with 12-bit dynamic range and sampling rates as high as 125 Msamples/s. Acquisition triggers are provided by the sync out signals from the laser *Q*-switch and US pulser/receiver.

The aforementioned light delivery probe is based on a confocal dark-field laser illumination approach, with some similarities to the dark-field PAM system first described by Maslov et al.[2] As shown in Fig. 2, an incident laser beam is reflected by a right angle prism which is mounted on an acrylic tube with refractive index of 1.46. The downward light is diverted by a polished reflective cone to a 25-deg polished surface of the tube. Then the reflected light travels downward along the tube and reaches another polished surface, which is machined at a certain angle to deflect the light confocally around the transducer focal axis. A 25-MHz single element ultrasound transducer (V324-SM, 12.7 mm focal length, Panametrics, Waltham, Massachusetts) is positioned inside the tube and can be adjusted vertically to match its focus point with the laser focus. In this design, light is focused at ∼10.5 mm below the bottom of the probe.

2.2 *Flow Phantom*

Experiments were performed on flow phantoms consisting of transparent vessels of 0.2- and 0.86-mm inner diameters (I.D.) embedded in a tissue-mimicking background. Polymer tubing (Paradigm Optics, Vancouver, Washington), composed of polyethylene terephthalate glycol (PETG) was used in construction of blood vessels. The inner diameters are representative of small arterioles and small veins.[8] The tissue-mimicking base was mixed with 10% cornstarch and 10% gelatin by weight, which offered an optical reduced scattering coefficient $\mu_s'=9.2\ \mathrm{cm}^{-1}$, similar to human tissues. The ultrasonic and mechanical properties are also within the range of typical biological tissues referred to previous work.[9]

Blood-mimicking fluid was pumped at mean flow velocities of 1 and 5 mm/s using a calibrated syringe pump (NE-300 Syringe Pump, New Era Pump Systems Inc., Eantagh,

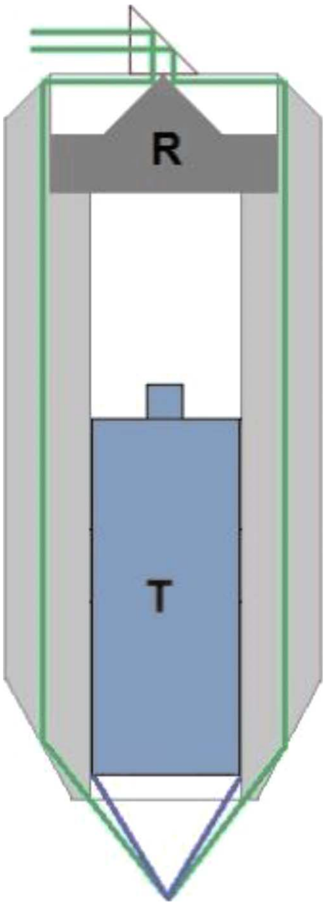

Fig. 2 Scheme of light delivery probe: R, reflective cone; T, US transducer.

New York). A 1-mm/s flow speed is thought to be typical in small vessels in the microcirculation. This is also a speed that begins to challenge our Doppler microultrasound system. We simply chose 5 mm/s as a speed significantly above 1 mm/s, and could be representative of flow in venules or arterioles.[8] The blood-mimicking fluid was composed of 5% by mass cornstarch dissolved in water, which ensures the blood to tissue signal power is consistent with *in vivo* signal levels. To increase the buoyancy of the particles, the mixture was first heated to 100 °C for several minutes and then cooled to room temperature before using. This fluid was also optically dyed by crystal violet to provide two optical absorption coefficients. One is $250\ \text{cm}^{-1}$ at 532 nm, the other is $3.3\ \text{cm}^{-1}$ at 630 nm, both of which are similar to human blood. The distance between the vessel and surface of the tissue phantom is 2 mm.

2.3 *Signal Processing Strategies*

PA and power Doppler US images are coregistered and superimposed on *B*-mode structural US images. To generate power Doppler images, steps in the signal processing chain involve signal alignment within and between lines of sight, wall filtering, Doppler power calculation, and thresholding.

In contrast to systems in which an ultrasonic pulse is repeatedly directed to a discrete line of sight, a swept-scan mode is used in our system to continuously scan over the flow phantom. The transducer is positioned over the region of interest, transmits one pulse and is laterally translated by one step within the pulse repetition period. This method can shorten the data acquisition time, but may cause signal decorrelations within each line of sight due to motion of the transducer. Three correlation-based alignment algorithms have been proposed for compensation purpose: single reference line, incremental, and averaging.[10] The first strategy selects a single pulse within a line of sight as reference and aligns other pulses by the relative shifts. The second calculates the relative shifts of consecutive pulses and aligns each pulse with the previous one. The third involves averaging the correlation over a set of reference lines. The nature of the swept-scan mode results in it being suitable for an incremental method. Within one line of sight, the relative shift of consecutive pulses is determined by finding the maximum of the cross-correlation estimate. In our case, interlaced PA signals may aggravate the discontinuities between lines of sight, thus we extend this incremental alignment method to better visualize blood vessel continuity. To perform alignment between lines of sight, the relative shift between the last pulse of one line of sight and the first pulse of the subsequent line of sight is first determined. Then the entire block of pulses within the subsequent line of sight is shifted by this determined amount.

Wall filters are necessary to reject strong clutter signals from surrounding tissues before Doppler power calculation. Typically an infinite impulse response (IIR) high-pass filter is used to remove slowly changing signals corresponding to tissue echoes. The limitation of such filters is that they have poor performance when Doppler frequencies generated by tissue motion exceed the cutoff frequencies. Thus, eigenfilters have been proposed to base the clutter filter on the statistics of the clutter signal so that the response can be adapted to the tissue movement. To address the fact that the clutter signal is a nonstationary random process, the discrete Karhunen-Loeve transform (DKLT) is used to characterize clutter signals.[11] It decomposes the autocorrelation matrix of received rf data into eigenvectors and eigenvalues, and then eigenvalues are sorted in decreasing amplitude. The eigenvalue spectrum is a generalization of the Fourier power spectrum, which represents the energy of the signal components. Thus, we can partition clutter signals, blood flow signals, and white noise by their eigenvectors according to this energy spectrum and eliminate the clutter noise by choosing appropriate filter order.

After wall filtering, the intensity of signals from moving blood is accumulated within each Doppler ensemble to generate power Doppler image. By a Doppler ensemble, we mean a sequence of N pulses, the echoes from which are processed to form one power Doppler A-scan line.

2.4 *Receiver Operating Characteristic Analysis*

Receiver operating characteristic (ROC) analysis can be used as a means of quantifying the performance of both power Doppler and PA imaging modes for the task of detecting blood (in our case blood-mimicking fluid). For each pixel in our images, we make a decision as to whether “blood” is present or absent. One way of making such a decision is to threshold the power Doppler or PA image. In practice, values above the threshold are color-coded (and thus classified as blood present) and the color-coded image is overlaid on a gray-scale US B-scan for structural context. By setting the threshold very low, a large number of color pixels may appear throughout the power Doppler (or PA) image due to noise, clutter, or other artifacts. Thus, a low threshold will yield a large fraction of true positives, but also a large number of false positives. A high threshold value may decrease the number of false positives, but at the expense of true positives. The trade-off between sensitivity and specificity can be graphically represented by an ROC curve that plots the true-positive fraction (TPF) versus the false-positive fraction (FPF) as the threshold level is varied from minimum to maximum. While we are interested ultimately in the estimation task of quantifying fractional blood volume in a region (which estimate can be thought of as the sum of the true positives and false positives), we note that thresholding can greatly impact this estimate. Moreover, to compare the performance of power Doppler and PA imaging modes, different threshold levels could be used for each mode. By comparing ROC curves for each mode (for different vessel sizes and flow conditions), we are able to objectively compare respective detection performances for the entire spectrum of possible threshold values. The area under the ROC curves (AROC) is used as a summary figure of merit to evaluate the detection performance of the two imaging modes.

3 Results

3.1 *Flow Phantom Experiments*

To demonstrate the performance of our combined system, flow phantoms with different vessel sizes were imaged by cross-sectional scans. Acoustic coupling was achieved by immersing flow phantoms in a water bath. The transducer was positioned so that the focus was 2 mm below the surface of the flow phantoms. The following acquisition settings were used in all experiments: 4-cycle pulse length, 39-dB receiver gain, and 16-μJ transmit energy. The motion controller was programmed to drive the voice coil scanning at a speed of 0.5 mm/s, which provides a distance of 25 μm between each line of sight. System specifications and experiment conditions are listed in Table 1. Scan speed and Doppler ensemble size are inversely related because the transducer is swept continuously during acquisition. The pulse repetition frequency (PRF) was set to 200 Hz when the laser was triggered at 20 Hz (the PRF was set to 100 Hz when the laser was triggered at 10 Hz), yielding a Doppler ensemble size of 10. When acquiring interleaved PA and Doppler signals, the trigger delay of the data acquisition card was set to 6 μs and the length of acquisition window was set to 20 μs, which enables a capture of 8.5-mm axial depth in both PA and power Doppler modes. The lateral distance of one scan trajectory was 10 mm. Interlaced data were separated to form individual PA, *B*-mode and power Doppler US images. Then PA and power Doppler images were coregistered and superimposed on the *B*-mode US images with structural contents.

Coregistered power Doppler and PA images acquired from the flow phantom with a 0.86-mm vessel diameter are shown in Figs. 3 and 4. Appropriate regions of interest (ROIs) are selected so that the blood volume fractions can be displayed in the center of the ROI. The ROI dimensions include a depth of 2.5 mm from top to bottom and a total lateral distance of 2.5 mm.

Table 1 System specifications and experiment conditions.

Parameters	Value
Transducer center frequency	25 MHz
Sampling frequency	100 MHz
Optical wavelengths	532 nm, 630 nm
Laser pulse repetition rate	20 Hz, 10 Hz
Doppler pulse repetition rate	200 Hz, 100 Hz
Ensemble size	10
Dynamic range	12 bits
Scan speed	0.5 mm/s
I.D. of vessels	0.86 mm, 0.2 mm
Flow velocities	5 mm/s, 1 mm/s
Eigenorder	1 to 4

Figure 3 shows power Doppler images acquired at mean flow velocities of 5 [Fig. 3(a)] and 1 mm/s [Fig. 3(b)], and coregistered PA images acquired at 532 nm [Fig. 3(c)]. In power Doppler mode, the cross section of blood vessel is well imaged at a high flow velocity [5 mm/s, Fig. 3(a)], but hard to interpret at 1 mm/s due to color pixel artifacts [Fig. 3(b)]. In PA mode, only the top surface can be well visualized because of the minimal light penetration depth in the vessel [Fig. 3(c)]. (Color online only.)

To show longer penetration depth in the PA image, we repeated our experiment on 0.86-mm flow phantom using a 630-nm wavelength. Figure 4 shows the PA image acquired at 630 nm [Fig. 4(c)] and coregistered power Doppler images [Fig. 4(a) and Fig. 4(b)]. In comparison to Fig. 3(c), Fig. 4(c) shows that a deeper penetration has been achieved, but the entire cross section of the vessel is still hard to see.

Figure 5 shows the coregistered power Doppler and PA images acquired from the flow phantom with a 0.2-mm vessel diameter. The ROI is 1.2×1.0 mm. The mean flow velocities are 5 [Fig. 5(a)] and 1 mm/s [Fig. 5(b)]. The optical wavelength is 532 nm. As shown in Figs. 5(a) and 5(b), power Doppler imaging has a good detection performance at a small vessel size (0.2 mm) and high flow velocity, but poor performance at slow flow velocity (1 mm/s). However, this small vessel can be easily detected in the PA image [Fig. 5(c)].

3.2 *Image Analysis*

Figure 6 shows ROC curves generated from both power Doppler and PA images at different vessel sizes, mean flow velocities, and optical wavelengths. Inspection of these individual ROC curves provides objective evaluation of blood flow detection performance of our combined system. Figure 6(a) shows the ROC analysis of power Doppler and PA images acquired at 0.86 mm I.D. and 532 nm. The color thresh-

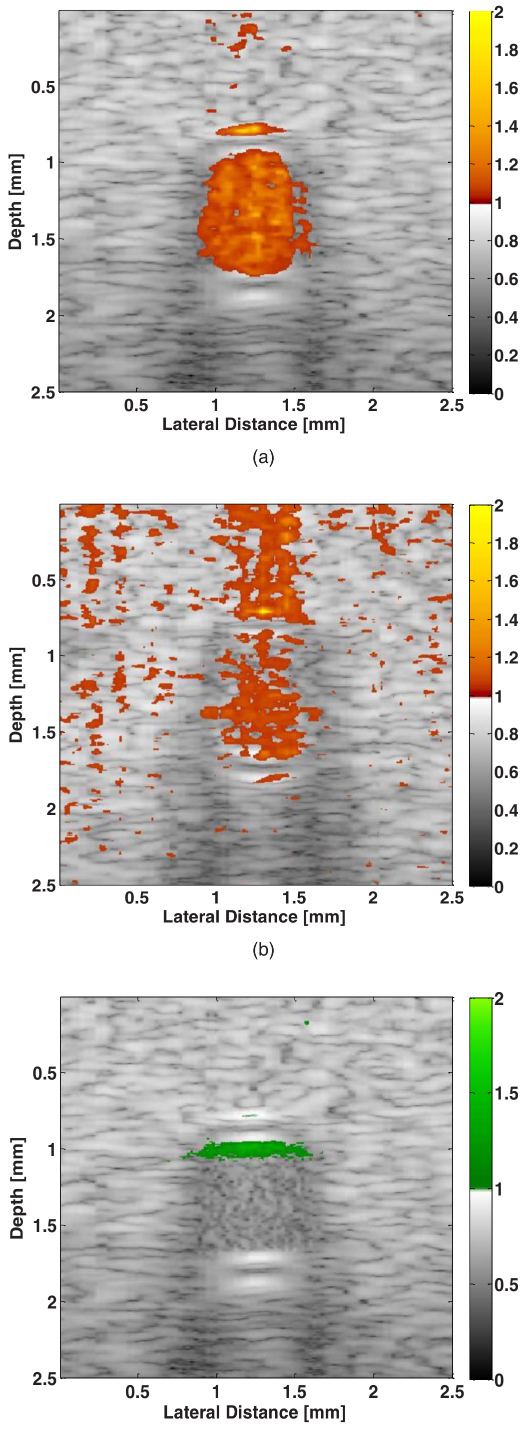

Fig. 3 Coregistered power Doppler and PA images of the flow phantom with a 0.86-mm vessel size: (a) power Doppler image at 5 mm/s, (b) power Doppler image at 1 mm/s, and (c) PA image at 532 nm.

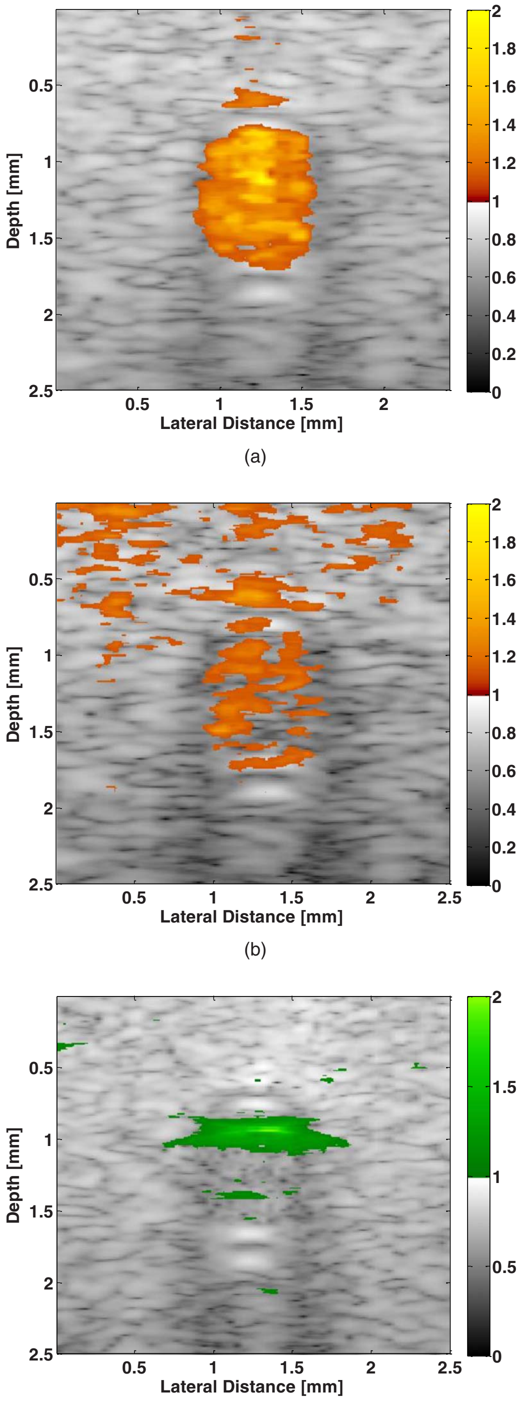

Fig. 4 Coregistered power Doppler and PA images of the flow phantom with a 0.86-mm vessel size: (a) power Doppler image at 5 mm/s, (b) power Doppler image at 1 mm/s, and (c) PA image at 630 nm.

olds are varied through the range of values, which ensures that the full ROC curve is populated. As shown in Fig. 6(a), the power Doppler image acquired at 5 mm/s produces an ROC curve that is consistently higher than the PA-ROC curve, indicating that power Doppler can provide a better estimation of blood volume fraction at 5 mm/s compared to the PA mode. The ROC curve generated from 1−mm/s power Doppler image moves close to a 45-deg diagonal line, which means that the detection accuracy and sensitivity decreases at low flow velocity. Figure 6(b) shows the ROC analysis of power Doppler and PA images acquired at 0.86 mm I.D. and 630 nm. The PA-ROC curve generated from 630 nm is higher than the one from 532 nm, which is due to the longer penetration depth. Figure 6(c) shows the ROC analysis when

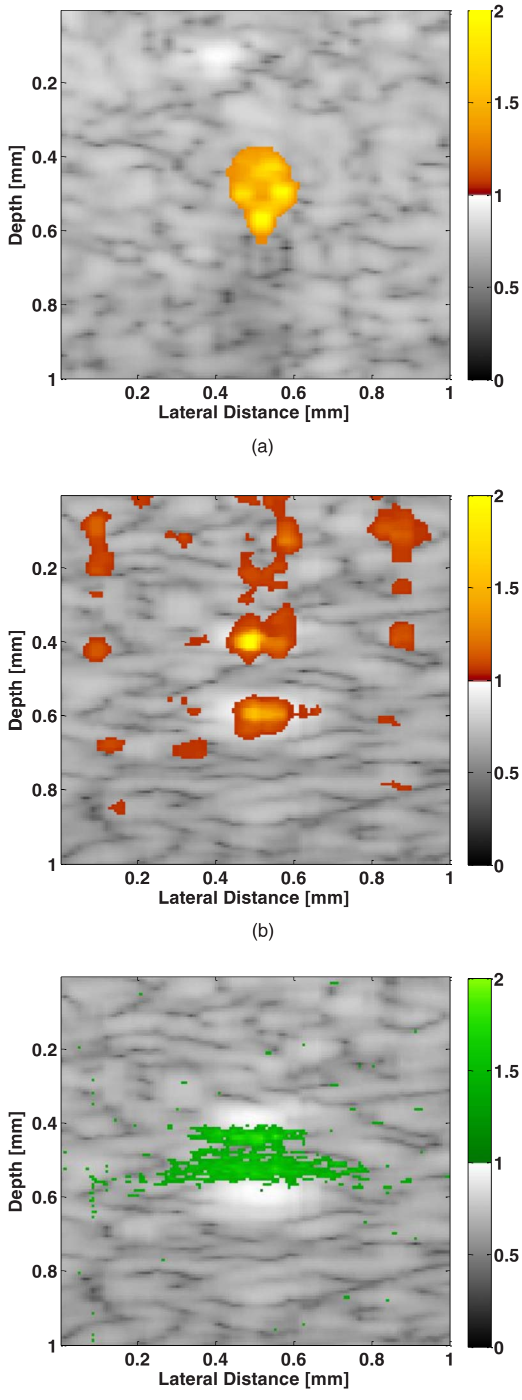

Fig. 5 Coregistered power Doppler and PA images of the flow phantom with a 0.2-mm vessel size: (a) power Doppler image at 5 mm/s, (b) power Doppler image at 1 mm/s, and (c) PA image at 532 nm.

the vessel diameter is 0.2 mm. While the ROC curve generated from the 1-mm/s power Doppler image lies almost along the diagonal line, the PA-ROC curve traverses through more of the upper left-hand quadrant of the ROC space. This is consistent with what we observe from the images, i.e., that PA imaging provides a better blood volume detection performance compared to power Doppler at small vessel size and slow flow velocity.

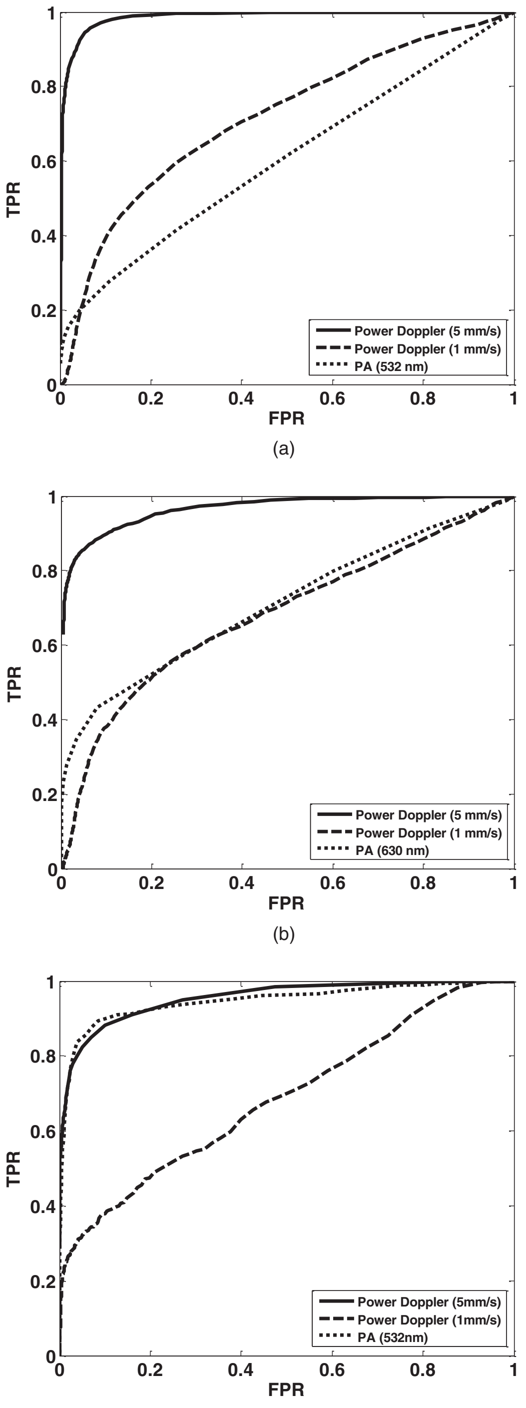

Fig. 6 ROC curves generated from PA and power Doppler images acquired at different vessel sizes and optical wavelengths: (a) 0.86 mm and 532 nm, (b) 0.86 mm and 630 nm, and (c) 0.2 mm and 532 nm. TPR, true positive rate; FPR, false positive rate.

The AROC values at different conditions are calculated using a trapezoidal rule and are shown in Table 2. When the vessel diameter is 0.86 mm, the AROCs demonstrate that good estimation of blood volume fraction, defined by AROC >0.90, can be achieved by power Doppler image at a high flow velocity (5 mm/s). For a small vessel size of 0.2 mm

Table 2 AROC for PA and power Doppler images.

	Optical Wavelength					
532 nm		630 nm			532 nm	
Vessel diameter	0.86 mm	0.86 mm	0.86 mm	0.86 mm	0.2 mm	0.2 mm
Mean flow velocity	5 mm/s	1 mm/s	5 mm/s	1 mm/s	5 mm/s	1 mm/s
Power Doppler	0.97	0.75	0.98	0.73	0.97	0.65
PA	0.63	0.64	0.79	0.76	0.95	0.93

and a slow flow velocity of 1 mm/s, the PA image has an AROC of 0.95, indicating a good performance of blood volume detection.

4 Discussion

To generate ROC curves, a circular region is fit so that the edges of the circle correspond to the maximum intensity points of the tubing innerwall in an US *B*-mode image. *In vivo*, there may not be such obvious wall signals, however, it provides us with a gold standard for a phantom study.

The ROC analysis demonstrates that power Doppler imaging has good detection performance for a large blood vessel (0.86 mm) and a high flow velocity (5 mm/s). However, the penetration depth of PA imaging may be limited at shorter wavelength (532 nm) so that it may not reveal the cross section of large blood vessel. Thus, a longer wavelength (630 nm) was used in this study [Fig. 4(c)]. The optical penetration depth is estimated as ~3 mm, which is much longer than the size of the vessel. However, even in this case, the entire cross section of the vessel cannot be well visualized in the PA image. Two key points might explain this: (1) light intensity will still decay appreciably in the vessel (the light intensity decay is estimated as ~25% by Beer's law) and (2) PA signals are bandpass filtered by the electromechanical response of the transducer. As such, absorption edges are seen better than slowly varying regions (which have low-frequency components). To explain this better, note that the PA image could be modeled as

$$\mathrm{PA}(x) = \mathrm{psf}(x)[\Gamma \mu_a(x)\Phi(x)],$$

where psf is the point-spread function, Γ is the Grueneisen parameter, μ_a is the optical absorption coefficient, and Φ is the local fluence. If the vessel is uniformly illuminated, Φ can be viewed as a constant. The psf, however, will have a bandpass response in the depth direction due to the electromechanical response of the transducer. Low spatial frequencies present in large absorbing structures may not survive bandpass filtering. Thus, obtaining good *B*-mode PA images of large vessels may be difficult due to the reasons already discussed (i.e., light penetration and the bandpass filtering response of the transducer). As shown in Fig. 4, even at 630 nm, power Doppler does outperform PA for a large vessel size (0.86 nm) and a high flow speed (5 mm/s). For a large a vessel size (0.86 mm) but a low flow velocity (1 mm/s), probably longer wavelength PA would be advantageous. A broadband transducer which has a wide frequency response can be used to compensate for the loss of lower acoustic frequencies due to bandpass filtering. Also, other Doppler methods such as interframe clutter filtering could be advantageous at the expense of power Doppler false positives associated with tissue motion artifacts.[12]

The ROC analysis also demonstrates that, for small blood vessel (0.2 mm), power Doppler imaging has good detection performance for a high flow velocity (5 mm/s), but poor performance for a slow flow velocity (1 mm/s). PA imaging has a good detection performance [Fig. 5(c)] for a small vessel, however, the lateral resolution and sidelobe levels of PA imaging may provide an undesirable FPR.

A combination of these two modalities offers advantages over either technique used alone. As no one set of power Doppler or PA parameters (pulse repetition rates, optical wavelengths, thresholds, etc.) will be successful at estimating fractional blood volume accurately for all vessels (large and small, high and low flow velocities), by understanding the relative merits of both techniques, it may be possible to improve our ability to estimate fractional blood volume by careful selection of PA or power Doppler parameters. This combined PA and Doppler US system is also capable of color Doppler imaging and sO_2 estimation. One long-term goal of our research is to use this system for noninvasive visualization of the metabolic rate of oxygen consumption (MRO_2) *in vivo*. MRO_2 is an important indicator of metabolic activities to diagnose cancer and diabetes. It is defined as the amount of oxygen consumed in a given tissue region per unit time per 100 g of tissue or of the organ of interest, and may be estimated in terms of the mean flow rate of vessels (mean flow velocity times vessel cross-sectional area), total concentration of hemoglobin C_{HB}, and the difference between the sO_2 of blood flowing into and out of a bounded tissue region.[13] Since mean flow velocity can be measured by color Doppler US, vessel cross-sectional area can be measured by power Doppler imaging or structural PA imaging, and functional PAM can be used to estimate sO_2 and C_{HB}, all of these parameters necessary for MRO_2 estimation can be provided by our combined system.

5 Conclusion

We developed a combined PA and high-frequency power Doppler US system that enables coregistered PA and power

Doppler images. Experiments were performed on flow phantoms with various combinations of vessel size, mean flow velocities, and optical wavelengths. ROC analysis was used to compare the detection performance of the PA and power Doppler imaging modes. Images with accompanying ROC analysis were presented. Work in progress involves color flow mapping and *in vivo* performance based on our combined system. Future work will develop multiwavelength PA microvessel imaging. With the ability to estimate blood flow velocity and oxygen saturation, we will devise estimators for computing metabolic rate of oxygen consumption.

Acknowledgment

We are grateful to Dr. Robert Fedosejevs for sharing his Nd:YAG laser. This research was sponsored by the Canadian Cancer Society (NCIC TFF 019237 and 019249), the Natural Sciences & Engineering Research Council of Canada (NSERC 355544-08), and the Canada Foundation for Innovation. We also acknowledge NSERC & iCORE student scholarships.

References

1. M. Xu and L. V. Wang, "Photoacoustic imaging in biomedicine," *Rev. Sci. Instrum.* **77**, 041101 (2006).
2. K. Maslov, G. Stoica, and L. V. Wang, "*In vivo* dark-field reflection-mode photoacoustic microscopy," *Opt. Lett.* **30**(6), 625–627 (2005).
3. H. F. Zhang, K. Maslov, G. Stoica, and L. V. Wang, "Functional photoacoustic microscopy for high-resolution and noninvasive *in vivo* imaging," *Nat. Biotechnol.* **24**, 848–851 (2006).
4. H. F. Zhang, K. Maslov, M. Sivaramakrishnan, G. Stoica, and L. V. Wang, "Imaging of hemoglobin oxygen saturation variations in single vessels *in vivo* using photoacoustic microscopy," *Appl. Phys. Lett.* **90**, 053901 (2007).
5. J. M. Rubin, R. O. Bude, P. L. Carson, R. L. Bree, and R. S. Adler, "Power Doppler US: a potentially useful alternative to mean frequency-based color Doppler US," *Radiology* **190**, 853–856 (1996).
6. J. A. Ketterling, O. Aristizábal, D. H. Turnbull, and F. L. Lizzi, "Design and fabrication of a 40-MHz annular array transducer," *IEEE Trans. Ultrason. Ferroelectr. Freq. Control* **52**(4), 672–681 (2005).
7. J. Folkman, "Angiogenesis: an organizing principle for drug discovery?" *Nat. Rev. Drug Discovery* **6**(4), 273–286 (2007).
8. S. Z. Pinter and J. C. Lacefield, "Detectability of small blood vessels with high-frequency power Doppler and selection of wall filter cut-off velocity for microvascular imaging," *Ultrasound Med. Biol.* **35**(7), 1217–1228 (2009).
9. R. J. Zemp, C. Kim, and L. V. Wang, "Ultrasound-modulated optical tomography with intense acoustic bursts," *Appl. Opt.* **46**(10), 1615–1623 (2007).
10. B. G. Zagar, R. J. Fornaris, and K. W. Ferrara, "Ultrasonic mapping of the microvasculature: signal alignment," *Ultrasound Med. Biol.* **24**(6), 809–824 (1998).
11. D. E. Kruse and K. W. Ferrara, "A new high resolution color flow system using an eigendecomposition-based adaptive filter for clutter rejection," *IEEE Trans. Ultrason. Ferroelectr. Freq. Control* **49**, 1739–1755 (2002).
12. A. Needle, D. E. Goertz, A. M. Cheung, and F. S. Foster, "Interframe clutter filtering for high frequency flow imaging," *Ultrasound Med. Biol.* **33**(4), 591–600 (2007).
13. L. V. Wang, "Prospects of photoacoustic tomography," *Med. Phys.* **35**(12), 5758–5767 (2008).